Theoretical analysis of the multiple-scattering contributions to the extended x-ray absorption fine-structure spectra at the barium L_1 and L_3 edges in BaF_2

1996 J. Phys.: Condens. Matter 8 5659

(http://iopscience.iop.org/0953-8984/8/30/015)

J. Phys.: Condens. Matter **8** (1996) 5659–5671. Printed in the UK

Theoretical analysis of the multiple-scattering contributions to the extended x-ray absorption fine-structure spectra at the barium L_1 and L_3 edges in BaF_2

Jesús Chaboy and Joaquin García

Instituto de Ciencia de Materiales de Aragón, CSIC—Universidad de Zaragoza, 50009 Zaragoza, Spain

Received 17 November 1995, in final form 15 April 1996

Abstract. In this work we present a detailed analysis of the extended x-ray absorption fine-structure (EXAFS) spectra at the barium L_1 and L_3 edges in BaF_2. Single-scattering (SS) and multiple-scattering (MS) contributions to the absorption spectra have been calculated for a unique cluster including contributions from atoms located up to 11 Å from the absorber. The combined analysis of both L_3- and L_1-edge EXAFS recorded at room temperature and at $T = 10$ K leads to the identification of several features appearing in the region extending over 2 and 6 $Å^{-1}$ as due to multiple-scattering effects. The contribution of the different MS paths to the EXAFS spectra is analysed carefully as a function of both the type of atom involved in the scattering process and the different MS geometries present in the BaF_2 structure.

1. Introduction

The analysis of the extended x-ray absorption fine-structure (EXAFS) part of the absorption spectra has been introduced as a structural tool in many interdisciplinary fields. The determination of reliable structural parameters from EXAFS requires a knowledge of backscattering amplitudes and phase shifts. In recent years, impressive progress has been made due to the development of first-principles methods, most of them based on multiple-scattering theory [1], for calculating the modulations of x-ray absorption spectra [2].

The relevance of multiple-scattering contributions to EXAFS spectra was for years the centre of intense debate. Nowadays, however, this debate has turned to the question of which class of MS contributions are relevant in EXAFS: is shadowing (focusing) the only important MS contribution in EXAFS or, in contrast, does non-collinear MS account for a significant fraction of the total amplitude?

In this investigation we have studied the extended EXAFS spectra at the barium L_1 and L_3 edges in BaF_2. The BaF_2 arrangement gives rise to a great number of multiple-scattering paths—both close to focusing geometry and non-collinear. Hence, the combined analysis of both the L_1 and the L_3 edges can clarify the influence of the MS contributions in the EXAFS part of the absorption spectra. With this aim we have performed theoretical *ab initio* multiple-scattering calculations of the different single-scattering (SS) and multiple-scattering (MS) contributions expected to be present in the EXAFS spectra. Our interest has been focused on determining which class of MS contributions are significant as regards modulating the amplitude and phase dependence of the EXAFS signals. The contribution of the different MS paths to the EXAFS spectra has been analysed as a function of both the

0953-8984/96/305659+13$19.50

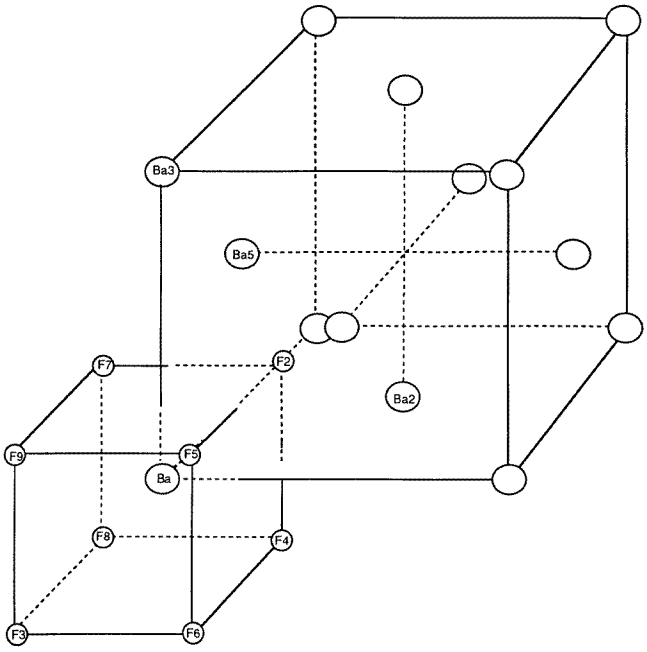

Figure 1. The crystallographic structure of BaF_2.

type of atom involved in the scattering process and the different MS geometries present in the BaF_2 structure.

2. Experimental details

X-ray absorption spectra at the Ba L edges were recorded for several BaF_2 samples at the Laboratory Nazionali di Frascati Synchrotron Radiation Facility using the PULS XAS station. The storage ring was operated at 1.5 GeV, the averaged current being approximately 40 mA, and the x-ray radiation was monochromatized using a Si(111) channel-cut crystal. The absorption data were collected at room temperature and $T = 10$ K in the transmission mode using two independent ionization chambers with the flowing gas mixture optimized for each energy range. Samples were prepared from crystalline BaF_2, which was finely ground and homogeneously spread on an adhesive tape clamped on a thick aluminium foil to ensure thermal homogeneity. Both the thickness and the homogeneity of the samples were optimized to obtain the best signal-to-noise ratio, giving a total absorption jump, $\Delta\mu x$, between 0.3 and 0.9.

Data analysis was carried out following the standard procedure [3]: the background contribution from previous edges $\mu_B(E)$ was fitted with a linear function and subtracted from the experimental spectrum $\mu(E)$. The post-edge absorption was fitted with a smooth spline formed by three cubic polynomials to simulate the atomic-like term $\mu_0(E)$. The EXAFS signal $\chi(k)$ was then determined as $\chi(k) = (\mu - \mu_B - \mu_0)/\mu_0$, where the photoelectron wave vector $\boldsymbol{k}$ is defined by $k = \sqrt{(2m/\hbar^2)(E - E_0)}$. At the L_1 edge, the energy origin, E_0, was defined to be at the inflection point of the absorption edge, while at the L_3 edge E_0 is located beyond the white line [4].

3. *Ab initio* EXAFS calculations

Theoretical computation of the EXAFS signals was performed at both the Ba L_1 and L_3 edges by using the multiple-scattering codes CONTINUUM and MSCALC, developed at the Laboratori Nazionali di Frascati, INFN-LNF by Natoli, Benfatto and co-workers [5, 6], and based on the one-electron full-multiple-scattering theory [1, 7, 8]. For the sake of brevity we avoid presenting here a detailed discussion of the theoretical methods used in the calculations, which can be found elsewhere [7, 9, 10, 11]. Therefore here we limit ourselves to summarizing the fundamental aspects of the computations. A full discussion of the procedure has been given previously in [11], where a detailed discussion about the approximations to multiple scattering, and the construction of the scattering potential, including the choices for the electron self-energy, is given.

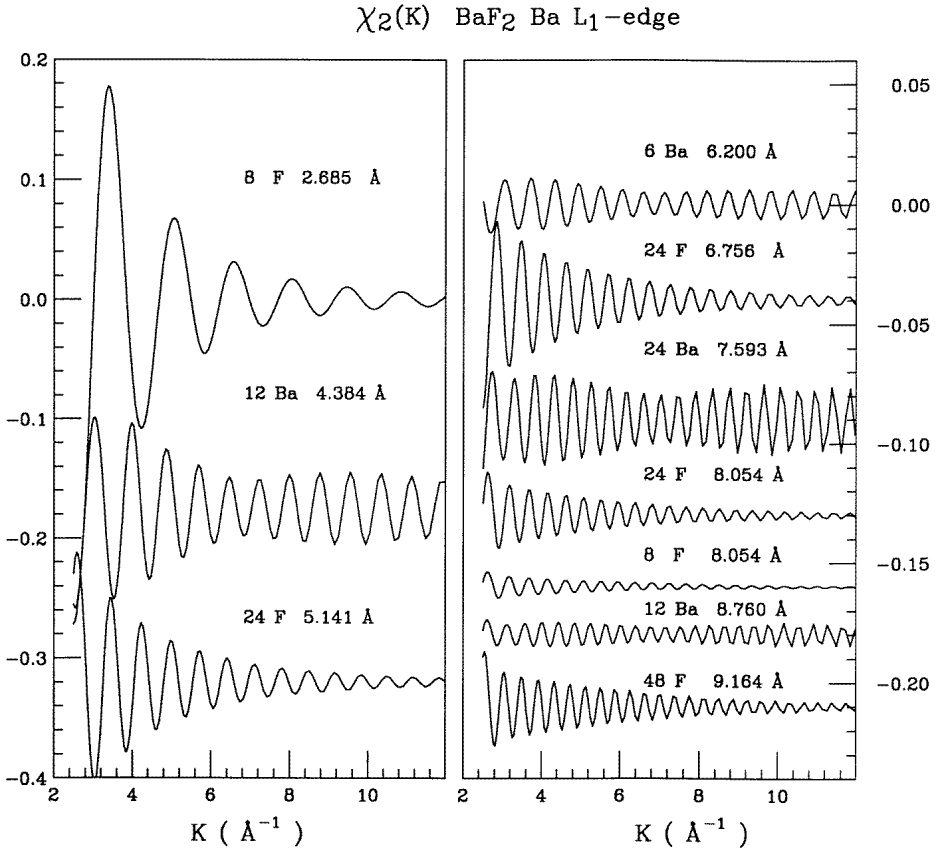

Figure 2. Theoretical Ba L_1-edge single-scattering signals calculated for the different coordination shells (see table 1) in the BaF_2 structure. (All of the signals are plotted using the same scale. The labels correspond to the signal at the top of the figure).

The cluster potential was built up starting from a set of spherically averaged muffin-tin (MT) potentials generated by standard methods [12], and by imposing a 10% overlap factor to the MT spheres whose radii were chosen following Norman's criterion [13]. The Coulomb part of each atomic potential was generated using charge densities for neutral

atoms obtained from tabulated atomic wave functions [14]. For the ground-state potential the atomic orbitals were chosen to be neutral, while for the excited-state potential the screened $Z + 1$ approximation was used. Finally, an exchange and correlation term was added to the Coulomb potential to actuate as the Dyson self-energy. The maximum angular momentum quantum number used in the EXAFS calculations was $l_{max} = 20$. In the case of the Ba L_3 edge, both d and s symmetry are allowed by the dipole selection rules for the final states involved in the absorption process. We have performed an explicit calculation of the EXAFS signals corresponding to the d $\leftarrow$2p and s $\leftarrow$2p excitation channels. The (d $\leftarrow$2p):(s $\leftarrow$2p) ratio has been found to be about 100. Therefore, we have neglected the s $\leftarrow$2p excitation channel in the theoretical simulation of Ba L_3-edge EXAFS spectra.

3.1. Single-scattering calculations

BaF_2 has the fluorite, CaF_2, cubic $Fm3m$ crystal structure. As shown in figure 1, the crystal cell can be described as formed of a barium sublattice in a cubic fcc arrangement, each barium atom being surrounded by a cube of eight fluorine atoms.

In a first step we have computed the single-scattering signals at both the Ba L_1 and L_3 edges for a BaF_2 cluster containing 239 atoms, i.e., covering an 11 Å region around the photoabsorbing barium. This cluster size was imposed taking advantage of the results obtained during the theoretical study of the XANES region of BaF_2 reported in a previous study [15, 16]. Indeed, the influence of the cluster size on both the phase and amplitude of the EXAFS signals is not negligible at low energies. For example, the amplitude of the EXAFS signal corresponding to the single scattering of the photoelectron by the nearest-neighbour shell calculated for a cluster containing the photoabsorbing Ba and eight F atoms in the first coordination shell is lower by a factor of 10% than that calculated for a cluster including up to five coordination shells, and, at the same time, the frequency of the EXAFS signal is found to be strongly sensitive to the choice of the cluster size [16]. Both effects are found to be non-negligible up to 5 Å^{-1} [16].

Moreover, in order to optimize the performance of the calculated EXAFS signals, we have studied the behaviour of the theoretical simulation upon imposing different exchange and correlation contributions to the scattering potential. This choice is found to be dramatic as regards obtaining a good agreement between the calculated and experimental spectra. The use of both X_α [17] and the energy-dependent Hedin–Lundqvist (HL) [18] potentials leads to a good agreement with the experimental data, while the use of the energy-dependent Dirac–Hara potential [19] leads to expanded EXAFS signals without one having to obtain reliable structural parameters. The reason for these differences can be traced back to the respective behaviours of the three potentials as functions of the energy. Indeed, the DH spectra tend to be expanded due to the rapid switching off of the exchange with the energy. It should be noted that the inadequacy of the DH potentials as regards accounting for the self-energy seems to be a general trend in the case of insulating materials. This effect has been pointed out in recent investigations regarding the XANES region of the absorption spectra [11, 16, 20]. The present study confirms this failure also for the high-energy region of the absorption spectra, in agreement with early predictions [21, 22].

Figure 2 shows the calculated single-scattering signals corresponding to the atomic distribution around the central Ba (see table 1) obtained using a 239-atom cluster. The EXAFS signal for both Ba L_1 and L_3 edges was then built up by adding the calculated single-scattering contributions for each coordination shell. In order to compare the calculated signals to the experimental data, we have performed a best-fitting procedure for the

Table 1. Atomic distribution around the central Ba in the BaF_2 structure. For each coordination shell, the coordination number, coordinates (cell parameter $a = 6.2$ Å), and the interatomic distance with respect to the absorbing Ba are given. On the right an identification for the shells (I), used in the discussion, is given.

Atom	N	x	y	z	Distance (Å)	I
Ba		0	0	0		
F	8	1/4	1/4	1/4	2.685	1F
Ba	12	1/2	1/2	0	4.384	1Ba
F	24	1/4	1/4	3/4	5.141	2F
Ba	6	1	0	0	6.200	2Ba
F	24	1/4	3/4	3/4	6.756	3F
Ba	24	1	1/2	1/2	7.593	3Ba
F	8	3/4	3/4	3/4	8.054	4F
F	24	5/4	1/4	1/4	8.054	5F
Ba	12	1	1	0	8.760	4Ba
F	48	5/4	3/4	1/4	9.164	6F

Table 2. Atomic coordinates of the fluorine atoms in the first coordination shell (1F) around the central Ba in the BaF_2 structure. The multiple-scattering paths calculated for the EXAFS simulations, shown in figure 4, are indicated together with their degeneracy.

Ba	0		0	0					
F2	1/4		1/4	1/4	F3	−1/4		−1/4	−1/4
F4	1/4		1/4	−1/4	F5	1/4		−1/4	1/4
F6	1/4		−1/4	−1/4	F7	−1/4		1/4	1/4
F8	−1/4		1/4	−1/4	F9	−1/4		−1/4	1/4
Multiple-scattering paths and degeneracy									
χ_3	F2–F3	8	F2–F4	24	F2–F6	24			
χ_4	F2–Ba–F2	8	F2–Ba–F3	8	F2–Ba–F4	24	F2–Ba–F6	24	
	F2–F3–F2	8	F2–F3–F4	48	F2–F3–F6	48	F2–F4–F2	24	
	F2–F4–F3	48	F2–F4–F5	96	F2–F4–F6	48	F2–F6–F2	24	
	F2–F6–F8	48							

experimental spectra and the total EXAFS signal calculated according to the expression

$$\chi_2(k) = \sum_j (N_j / k R_j^2) |F_j(k, R_j)| \sin(2kR_j + \Psi_j(k)) e^{-2k^2\sigma_j^2} e^{-2R_j/\lambda(k)}. \qquad (1)$$

The sum extends over the various shells surrounding the central atom, and R_j, N_j and σ_j^2 are, respectively, the distances, the coordination numbers, and the mean square vibrational amplitude for each shell distance. $|F_j(k, R)|$ is the backscattering amplitude of the neighbouring atoms, and $\Psi(k)$ accounts for the total phase shift probed by the photoelectron in the scattering path due to both the central and neighbouring atoms. Finally, λ is the mean free path of the photoelectron.

The computation of all the single-scattering signals, performed by using the same big cluster for the potential and phase-shift calculations, provides advantages additional to those mentioned above—in particular the reduction of the number of free parameters in the fitting process. Indeed, the effective mean free paths λ for both edges have been calculated from the imaginary part of the HL ECP in which the proper core-hole lifetime for each absorption edge ($\Gamma_{L_3} = 3.2$ eV, $\Gamma_{L_1} = 4.5$ eV) has been included. Also, because the scattering signals

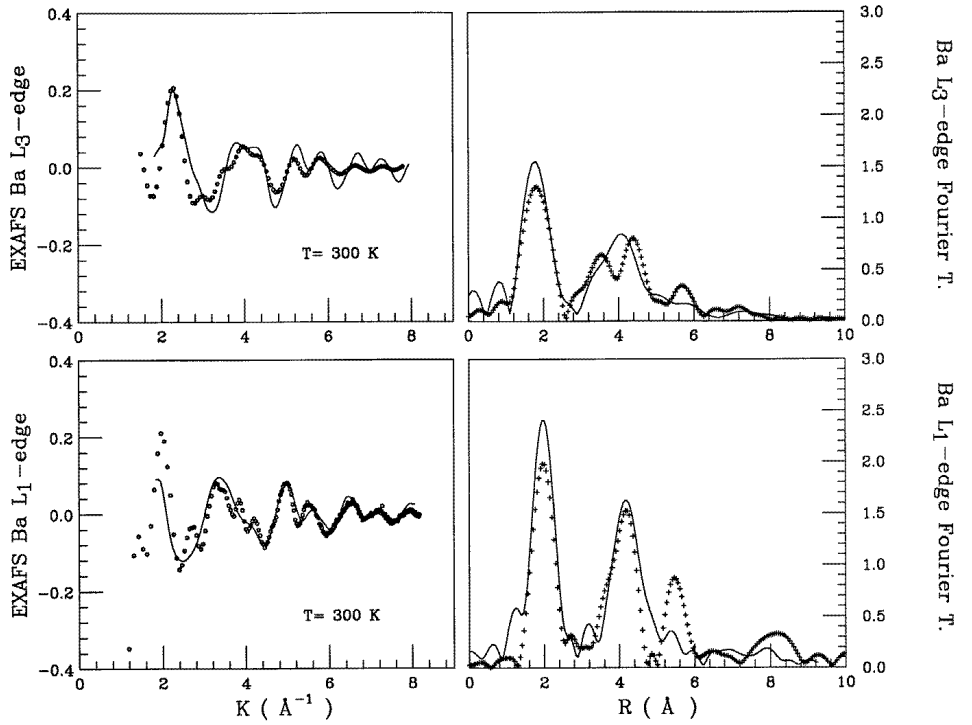

Figure 3. A comparison between the experimental Ba L_1- and L_3-edge EXAFS spectra and their Fourier transforms for BaF_2 recorded at room temperature (dots) and the theoretical simulation including the single-scattering signals calculated for the different coordination shells shown in figure 2 (solid line).

have been calculated using the same cluster, i.e., the same potential, the EXAFS signals for each coordination shell are referred to a unique zero energy. Moreover, the comparison of the XANES spectra and theoretical computations at both the L_1 and L_3 edges performed in [16] provides the shift in energy, E_0, needed to match the near-edge peaks. Hence, both λ and E_0 have been kept fixed during the refinement process. Moreover, as we deal with a known crystalline structure, coordination numbers are also fixed. Consequently, during the best-fitting process the parameters that were allowed to vary are the interatomic distances and the mean square displacement, σ^2. However, in our analysis we have also taken advantage of having experimental data at both room temperature and $T = 10$ K. In this way, we have Fourier transformed the experimental data in the k-range $1.5 \leqslant k \leqslant 8.5$ Å^{-1} and Fourier filtered the first-shell contribution in the R-ranges $0.4 \leqslant R \leqslant 3$ and $0.8 \leqslant R \leqslant 3.2$ Å for the L_1 and L_3 edges, respectively. The EXAFS signals for the low-temperature phase obtained in this way were fitted to those of the spectra recorded at room temperature according to equation (1) and allowing the variation of both R and σ^2. This procedure yields to a relative decrease of 0.004 Å^2 and 0.017 Å for the mean square displacement and the interatomic distance, respectively, of the low-temperature EXAFS signal. This relative variation was then incorporated as a boundary condition into the fitting of the calculated EXAFS signals and the experimental spectra, which was then carried out simultaneously for the two working temperatures.

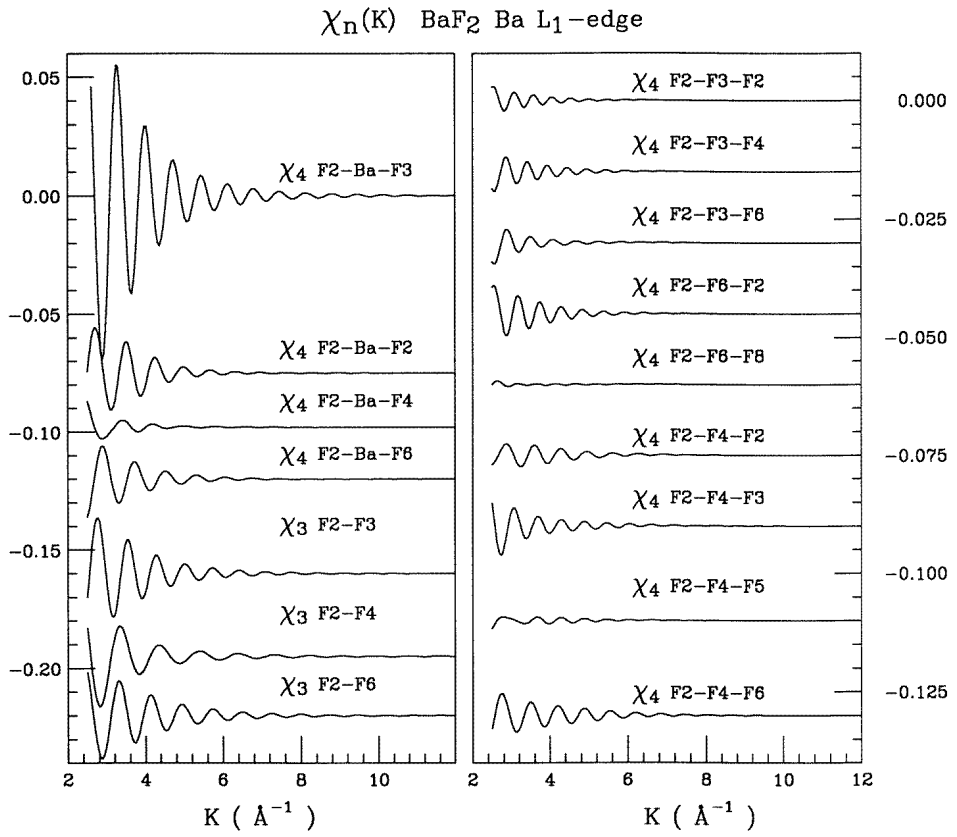

Figure 4. Calculated Ba L_1-edge multiple-scattering contributions coming from photoelectron paths within the first fluorine coordination shell around the central Ba in BaF_2. The labels of the different atoms refer to table 2 and are shown in figure 1. (All of the signals are plotted using the same scale. The labels correspond to the signal at the top of the figure.)

The comparison of the experimental EXAFS signals and the theoretical simulation obtained according to equation (1) by using the parameters summarized in table 4 is shown in figure 3. The computation reproduces well the experimental spectra in the high-energy region ($k \geqslant 5$ Å^{-1}) at both the L_1 and L_3 edges, but the agreement in the low-energy region is unsatisfactory. Despite the main frequency of the EXAFS signals being qualitatively reproduced, there are several features in the range $2 \leqslant k \leqslant 5$ Å^{-1} that are not reproduced by the calculation. Moreover, the interatomic distances derived for the third and fourth coordination shells are very far from reproducing the crystallographic values. These results are found in a similar way for the experimental spectra at both absorption edges, and independently of the temperature. This trend points out the existence of additional contributions to the EXAFS spectra that we are not considering. Indeed, inspection of the Fourier transforms shown in figure 3 indicates the existence of two contributions centred at about 5.5 and 8 Å that are not reproduced by the theoretical calculation. Moreover, the agreement in the region $2.5 \leqslant R \leqslant 5.5$ Å, which is expected to arise from scattering processes involving the second and third coordination shells, is far from being accounted for by the computation.

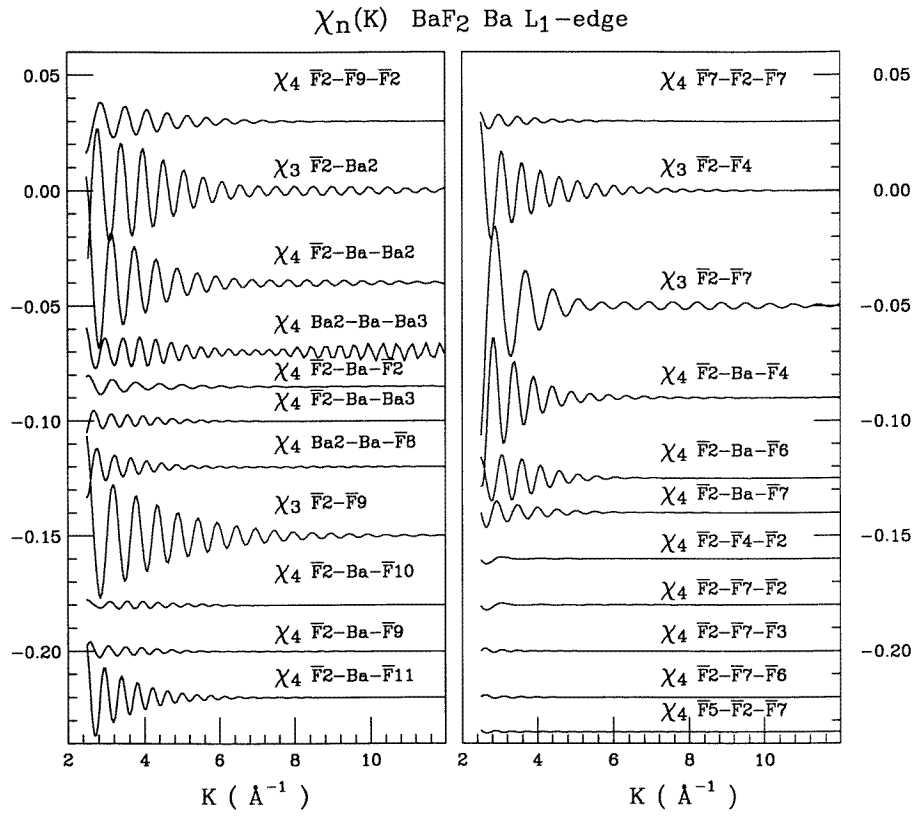

Figure 5. Calculated Ba L_1-edge multiple-scattering paths involving atoms of the coordination shells 1F–1Ba, 1F–2F, 1F–3F and 1Ba–2F. The coordinates of the atoms involved in the scattering paths and the degeneracy of each path are given in table 3.

3.2. Multiple-scattering calculations

The discrepancies found in the *ab initio* single-scattering analysis of the absorption data have to be attributed to the existence of non-negligible multiple-scattering contributions in the experimental EXAFS spectra. We thus proceeded to compute the contribution to the EXAFS signals at both the Ba L_1 and L_3 edges of the different MS processes occurring in the BaF_2 structure.

The number of MS paths in this crystalline structure involving scattering processes within an 11 Å sphere around the central Ba is so high that the full calculation would be a very hard task. In order to avoid this computational problem we have proceeded using a two-step method. First, we have computed all of the MS contributions, χ_3 and χ_4, involving the photoabsorbing Ba and the eight fluorine atoms of the first coordination shell, as indicated in table 2. The number of such processes is 512, distributed as three different χ_3- and thirteen χ_4-paths with total degeneracy 56 and 456, respectively. The result of this calculation at the Ba L_1 edge is shown in figure 4. The most intense contribution is associated with the F2–Ba–F3 χ_4-path in which the central barium also actuates as a scatterer in the focusing geometry. Although the same linear arrangement is present in the F2–F3 χ_3-path, the amplitude of the signal is only half of the former. This difference

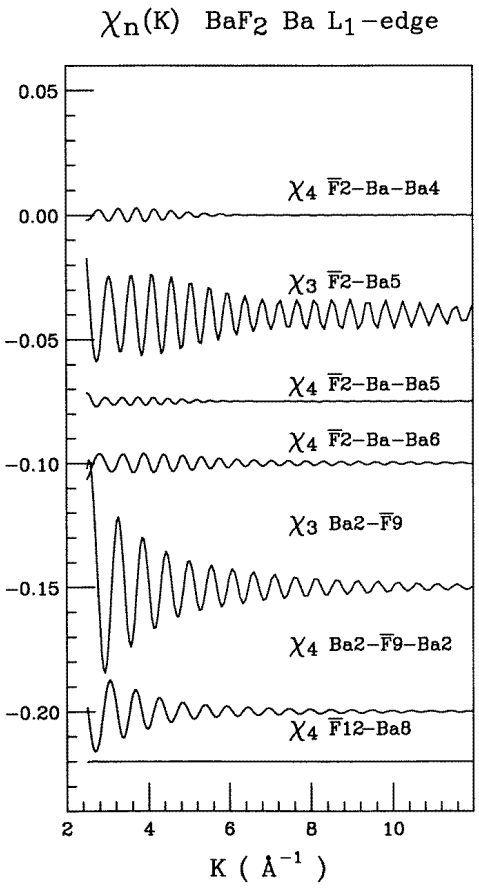

Figure 6. Calculated Ba L_1-edge multiple-scattering paths involving atoms of the coordination shells 1Ba–3F, 1F–2Ba, 2F–3Ba and 1F–3Ba. The coordinates of the atoms involved in the scattering paths and the degeneracy of each path are given in table 3.

can be attributed to the critical role played by the barium atom. Indeed, the amplitude of all of the MS signals involving Ba in the scattering path is significantly greater than that associated with χ_4-paths in which the middle atom is F instead of Ba. Moreover, contrary to the extended supposition that only focusing scattering paths (FSP) contribute significantly to the EXAFS spectra, we find that the amplitudes of the MS χ_3- and the F2–Ba–F6 MS χ_4-signals in non-linear geometry are comparable to that of the FSP, and therefore their contribution to the EXAFS spectra is not negligible. Also the different k-dependences of the MS signals calculated for identical paths at both the L_1 and L_3 edges should be noted. This effect is the expected consequence of the different phase shifts associated with the absorbing atom in both 1s- and 2p-electron excitations, as previously discussed in [4].

These results provide us with a criterion for reducing the number of MS signals to be calculated for scattering paths involving atoms beyond the nearest-neighbour fluorine shell. We have limited our calculation to MS paths contained within the first six coordination shells, i.e., covering a region of 7.6 Å around the absorbing Ba. Therefore we have calculated: χ_4-paths in which a barium atom—not necessarily the absorbing one—is in the middle of

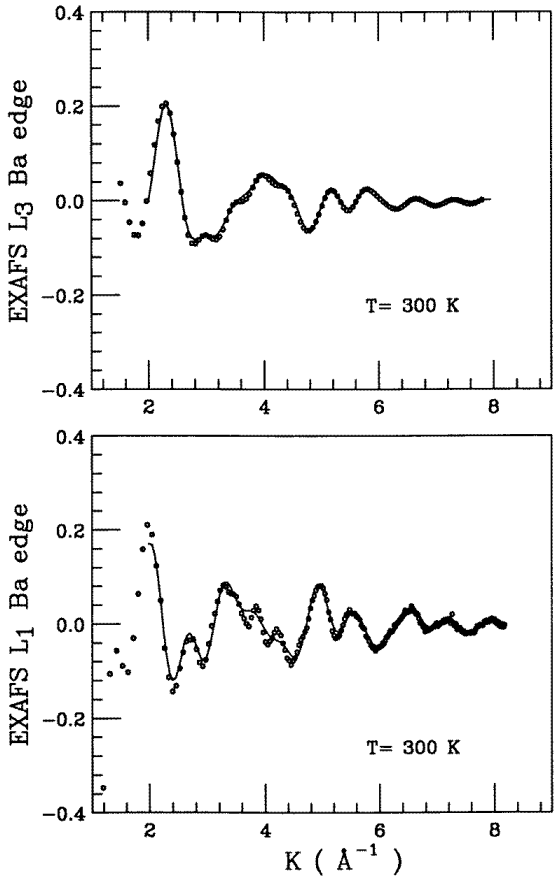

Figure 7. A comparison between the experimental Ba L_1- and L_3-edge EXAFS spectra and the theoretical simulation including both the calculated single- and multiple-scattering contributions.

the chain, linear or not; χ_3-paths in both non-collinear and collinear configurations; and, finally, and for the sake of comparison, fluorine χ_4-chains in focusing geometry. The list of the calculated paths is given in table 3 and the associated signals are reported in figures 5 and 6 (for the sake of brevity only the L_1 signals are shown in figure 5). There are three groups of MS paths found to present an amplitude comparable to or even higher than, for example, the single-scattering contribution of the six Ba atoms located a 6.2 Å from the absorber; see figure 2: the χ_4-paths in which Ba is in the middle of the chain; and χ_3-paths, both linear and not, involving two fluorine atoms or one fluorine and one barium atom. In particular, this last class of paths presents an amplitude that is not negligible even at high k.

In order to visualize the relative importance of both single- and multiple-scattering contributions to the EXAFS spectra, we have added all of the calculated MS signals and compared the Fourier transform of this sum to that of the experimental spectra. Beyond the first coordination shell multiple scattering is not negligible. Moreover, the peak at about 5.5 Å is well reproduced by the calculation. Also, a significant contribution of the MS is found to be present in the FT region extending from 2.5 to 5.5 Å, i.e., in the region where

Table 3. Calculated multiple-scattering paths involving atoms beyond the first coordination sphere around the central Ba in the BaF_2 structure. The coordinates of the different atoms are given together with the degeneracy of each path. The result of the computation is shown in figure 5 and figure 6.

Ba2	1/2	1/2	0	Ba3	0	0	1
Ba4	0	0	−1	Ba5	1	1/2	1/2
Ba6	−1/2	−1	−1/2	Ba7	−1/2	1/2	−1
Ba8	−1	1/2	1/2	$\bar{F}2$	1/4	1/4	1/4
$\bar{F}3$	1/4	1/4	−3/4	$\bar{F}4$	−1/4	−1/4	−3/4
$\bar{F}5$	3/4	−1/4	−1/4	$\bar{F}6$	1/4	−1/4	−3/4
$\bar{F}7$	1/4	1/4	3/4	$\bar{F}8$	−3/4	−1/4	−1/4
$\bar{F}9$	3/4	3/4	1/4	$\bar{F}10$	1/4	−3/4	−3/4
$\bar{F}11$	−3/4	−3/4	−1/4	$\bar{F}12$	−3/4	1/4	1/4

Multiple-scattering $\chi_{3,4}$-paths and degeneracy

1F–1Ba	$\bar{F}2$–Ba2	6					
	$\bar{F}2$–Ba–Ba2	6	$\bar{F}2$–Ba2–$\bar{F}2$	3	$\bar{F}2$–Ba2–Ba3	6	
1F–2F	$\bar{F}2$–$\bar{F}4$	6	$\bar{F}2$–$\bar{F}7$	6			
	$\bar{F}2$–Ba–$\bar{F}4$	6	$\bar{F}2$–Ba–$\bar{F}6$	12	$\bar{F}2$–Ba–$\bar{F}7$	6	
	$\bar{F}2$–$\bar{F}4$–$\bar{F}2$	3	$\bar{F}2$–$\bar{F}7$–$\bar{F}2$	3	$\bar{F}2$–$\bar{F}7$–$\bar{F}3$	6	
	$\bar{F}2$–$\bar{F}7$–$\bar{F}6$	12	$\bar{F}5$–$\bar{F}2$–$\bar{F}7$	12	$\bar{F}7$–$\bar{F}2$–$\bar{F}7$	3	
1Ba–2F	Ba2–Ba–$\bar{F}8$	8					
1F–3F	$\bar{F}2$–$\bar{F}9$	6	$\bar{F}2$–Ba–$\bar{F}10$	6			
	$\bar{F}2$–Ba–$\bar{F}9$	6	$\bar{F}2$–Ba–$\bar{F}11$	6	$\bar{F}2$–$\bar{F}9$–$\bar{F}2$	3	
1Ba–3F	Ba2–$\bar{F}9$	4	Ba2–$\bar{F}9$–Ba2	2			
1F–2Ba	$\bar{F}2$–Ba–Ba4	6					
2F–3Ba	$\bar{F}2$–$\bar{F}12$	2					
1F–3Ba	$\bar{F}2$–Ba5	6	$\bar{F}2$–Ba–Ba5	6	$\bar{F}2$–Ba–Ba6	4	

the single-scattering theoretical calculations fail to reproduce the experimental data.

As a final step, we have performed the structural analysis as in the preceding section but now taking into account the MS contributions. However, instead of introducing as a fitting parameter in the refinement process the interatomic distances and the mean square displacements for each MS path, thus considerably increasing the number of free parameters, we have returned to the following approximation: we have Fourier filtered the MS contribution in the ranges $2 \leqslant R \leqslant 4.9$ and $4.9 \leqslant R \leqslant 6.2$ for the L_3 case ($2.8 \leqslant R \leqslant 5.6$ and $5.6 \leqslant R \leqslant 6.8$ for the L_1 case) so that it acts as two effective MS signals to be included in the fitting process in the same manner as the single-scattering signals. The condition on the relative variation of the mean square displacements between the spectra at room and low temperature has also been included for the effective MS signals, with the additional constraint that in no case can the σ^2-factor associated with the MS signal be lower than those of the single-scattering signals associated with the atoms involved in the MS paths. The comparison of the theoretical signals obtained at both the Ba L_1 and L_3 edges obtained according to this procedure by using the parameters summarized in table 4 and the experimental EXAFS spectra is reported in figure 7. As shown in the figure, despite the strong approximations involved, the experimental data are well reproduced by the calculation. In particular, the interatomic distances derived for the third and fourth coordination shell are now close to the crystallographic values, and the absorption features present in the range $2 \leqslant k \leqslant 5$ Å^{-1} that were absent in the single-scattering computation are now well reproduced.

Table 4. Coordination numbers, interatomic distances and Debye–Waller parameters obtained from the comparison of the experimental spectra and the single-scattering theoretical simulations for both Ba L_1 and L_3 edges in BaF_2. At the bottom, the results shown have been obtained including the multiple-scattering contributions as described in the text.

Atom	N	XRD R (Å)	10 K R (Å)	10 K σ^2 (Å^2)	300 K R (Å)	300 K σ^2 (Å^2)
Ba L_1-edge single scattering						
F	8	2.685	2.670	0.0014	2.670	0.0066
Ba	12	4.384	4.404	0.0010	4.388	0.0008
F	24	5.141	5.261	0.0010	5.260	0.0014
Ba	6	6.200	5.570	0.0028	5.561	0.0072
Ba L_3 edge						
F	8	2.685	2.670	0.0014	2.672	0.0047
Ba	12	4.384	4.372	0.0035	4.349	0.0091
F	24	5.141	5.253	0.0019	5.270	0.0105
Ba	6	6.200	6.027	0.00001	6.600	0.00002
Ba L_1-edge single and multiple scattering						
F	8	2.685	2.670	0.0014	2.670	0.0063
Ba	12	4.384	4.404	0.0015	4.388	0.0070
F	24	5.141	5.150	0.0017	5.161	0.0090
Ba	6	6.200	6.220	0.0026	6.210	0.0100
Ba L_3 edge						
F	8	2.685	2.670	0.0014	2.672	0.0047
Ba	12	4.384	4.424	0.0068	4.421	0.0122
F	24	5.141	5.149	0.0078	5.133	0.0183
Ba	6	6.200	6.242	0.0238	6.264	0.0326

4. Summary and conclusions

We have reported in the present work the analysis of the extended x-ray absorption fine-structure (EXAFS) spectra at the barium L_1 and L_3 edges in BaF_2. This analysis has been conducted to discern the relative importance of single-scattering and (SS) and multiple-scattering (MS) contributions to the absorption spectra.

The comparison between the experimental data at the two edges and different XAS-MS calculations has demonstrated the need to use large clusters to obtain a good reproduction of the experimental spectra. The cluster size used to generate the scattering potential influences the phase and amplitude of the EXAFS signals at low energies. For the exchange and correlation contributions to the scattering potential, we have found that the best agreement with the experimental data is achieved by using the energy-dependent Hedin–Lundqvist (HL) potential. In contrast, the use of the energy-dependent Dirac–Hara potential produces expanded EXAFS signals, and no reliable structural determination can be produced.

The analysis performed by considering exclusively SS contributions to the experimental EXAFS has been found to be inadequate at both the barium L_1 and L_3 edges. Indeed, only when including the MS contributions is it possible to obtain a good agreement between the theoretical simulation and the experimental spectra. We have devoted special attention to discerning which are the most important MS paths contributing to the absorption spectra. Our findings reveal—contrary to previous assignments [23]—that the amplitude of the MS signals depends more on the nature of the scatterer than on the existence of collinear

arrangements giving rise to focusing processes. Indeed, we have identified as the most intense contributions to the EXAFS those arising from χ_4-paths in which a barium atom is in the middle of the chain even when it is not collinear. In contrast, collinear arrangements of fluorine atoms do not contribute significantly to the EXAFS. Moreover, also χ_3-paths in non-collinear configuration have been found to be non-negligible, in particular when barium is present in the chain.

Acknowledgments

This work was partially supported Diputación General de Aragón DGA PCB09-93, Spanish CICYT MAT93-0240C04 and PB92-1077 grants, and by the INFN-CICYT agreement. We wish also to acknowledge A Marcelli, C R Natoli and M Benfatto for many friendly and fruitful discussions.

References

[1] Lee P A and Pendry J B 1975 *Phys. Rev.* B **11** 2795
[2] Vvedensky D D, Saldin D K and Pendry J B 1986 *Comput. Phys. Commun.* **40** 421
Durham P J, Pendry J B and Hodges C H 1986 *Comput. Phys. Commun.* **40** 421
Natoli C R and Benfatto M, unpublished
Binsted N, Gurman S J and Campbell S, unpublished
Rehr J J, Mustre de Leon J, Zabinsky S I and Albers R C 1991 *J. Am. Chem. Soc.* **113** 5315
Mustre de Leon J, Rehr J J, Zabinsky S I and Albers R C 1991 *Phys. Rev.* B **44** 4146
[3] Lengeler B and Eisenberger P 1980 *Phys. Rev.* B **21** 4507
[4] Chaboy J, García J and Marcelli A 1992 *Solid State Commun.* **82** 939
[5] Natoli C R and Benfatto M 1987 *INFN Laboratori Nazionali di Frascati, CONTINUUM program*
[6] Natoli C R, Benfatto M and Tyson T A 1989 *INFN Laboratori Nazionali di Frascati, MSCALC program*
The updated version of this code is known as MSXAS.
Ruiz-Lopez M F, Bohr F, Filipponi A, Di Cicco A, Tyson T A, Benfatto M and Natoli C R 1991 *X-ray Absorption Fine Structure* ed S S Hasnain (Chichester: Ellis Horwood) p 75
[7] Natoli C R and Benfatto M 1986 *J. Physique Coll.* **47** C8 11
[8] Lee P A and Pendry J B 1977 *Phys. Rev.* B **15** 2862
[9] Benfatto M 1990 *2nd European Conf. on Progress in X-ray Synchrotron Radiation Research* ed A Balerna, E Bernieri and S Mobilio (Bologna: Societá Italiana di Fisica) p 3
[10] Tyson T A, Hodgson K O, Natoli C R and Benfatto M 1994 *Phys. Rev.* B **46** 5997
[11] Chaboy J and Quartieri S 1995 *Phys Rev.* **52** 6349
[12] Mattheis L F 1964 *Phys. Rev.* A **133** 1399; 1964 *Phys. Rev.* A **134** 970
[13] Norman J G 1974 *Mol. Phys.* **81** 1191
[14] Clementi E and Roetti C 1974 *At. Data Nucl. Data Tables* **14** 177
[15] Chaboy J 1996 *Solid State Commun.* at press
[16] Chaboy J 1991 *PhD Thesis* University of Zaragoza
[17] Slater J C 1979 *The Self-Consistent Field for Molecules and Solids; Quantum Theory of Molecules and Solids* (New York: McGraw-Hill)
[18] Hedin L and Lundqvist B I 1971 *J. Phys. C: Solid State Phys.* **4** 2064
[19] Hara S 1967 *J. Phys. Soc. Japan* **22** 710
[20] Chaboy J, Benfatto M and Davoli I 1995 *Phys Rev.* B **52** 10 014
[21] Sainctavit P, Petiau J, Benfatto M and Natoli C R 1990 *Proc. 2nd European Conf. on Progress in X-ray Synchrotron Radiation Research (Rome, 1989)* ed A Balerna, E Bernieri and S Mobilio (Bologna: Editrice Compositori) p 31
[22] Rehr J J 1991 *X-ray Absorption Fine Structure* ed S S Hasnain (Chichester: Ellis Horwood) p 15
[23] Kuzmin A, Purans J, Benfatto M and Natoli C R 1993 *Phys. Rev.* B **47** 2480